

Effect of *n*-Butanol Cofeeding on the Methanol to Aromatics Conversion over Ga-Modified Nano H-ZSM-5 and Its Mechanistic Interpretation

Weili Dai,^{†,‡,§} Liu Yang,[†] Chuanming Wang,[§] Xin Wang,[†] Guangjun Wu,^{†,‡} Naijia Guan,^{†,‡} Utz Obenaus,^{||} Michael Hunger,^{||} and Landong Li^{*,†,‡,§}

[†]School of Materials Science and Engineering & National Institute for Advanced Materials, Nankai University, Tianjin 300350, P. R. China

[‡]Key Laboratory of Advanced Energy Materials Chemistry of the Ministry of Education, Collaborative Innovation Center of Chemical Science and Engineering, Nankai University, Tianjin 300071, P. R. China

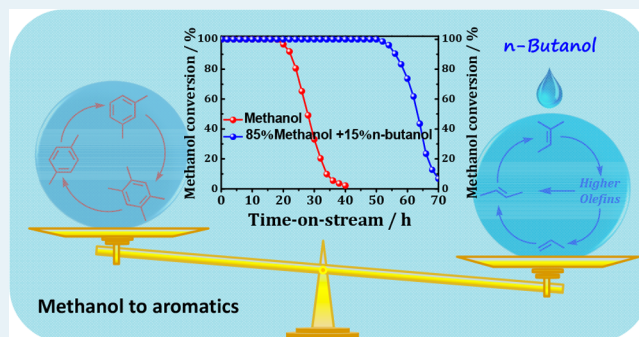
[§]SINOPEC Shanghai Research Institute of Petrochemical Technology, Shanghai 201208, P. R. China

^{||}Institute of Chemical Technology, University of Stuttgart, 70550 Stuttgart, Germany

Supporting Information

ABSTRACT: Ga-modified nano H-ZSM-5 zeolites with different Ga contents were prepared and applied as methanol-to-aromatics (MTA) catalysts. The Ga introduction can strongly increase the selectivity to aromatics but also decrease the catalyst lifetime simultaneously. Upon the cofeeding of *n*-butanol with methanol, a significant prolongation of the catalyst lifetime from 18 to ca. 50 h can be achieved. According to several spectroscopic results, e.g., TGA, GC–MS, in situ UV/vis, and solid-state MAS NMR spectroscopy, the addition of *n*-butanol during the MTA conversion shows no impact on the deactivation mechanism but can influence the dual-cycle mechanism. Namely, *n*-butanol preferentially adsorbs on Brønsted acid sites over methanol, followed by dehydration into *n*-butene. The formed *n*-butene can directly participate in the olefin-based cycle and, therefore, significantly alter the proportions of the dual-cycle mechanism. These results provide mechanistic insights into the roles of *n*-butanol cofeeding in the MTA conversion and exemplify a simple but efficient strategy to prolong the catalyst lifetime, which is crucial to the industrial application.

KEYWORDS: ZSM-5, gallium modification, methanol-to-aromatics, dual-cycle mechanism, prolonged catalyst lifetime



1. INTRODUCTION

The conversion of methanol to hydrocarbons (MTH) over acidic zeolite catalysts has attracted significant attention since its discovery in 1977.^{1–10} Many fuels and chemicals, e.g., gasoline, olefins, and aromatics, can be produced according to this process. Among these products, aromatics, especially benzene, toluene, and xylenes, known as BTX, are the most important raw chemicals for the production of synthetic rubbers, perfumery, and medicine.^{11–14} Traditionally, aromatics production is based on the petroleum route, e.g., naphtha reforming and oil cracking. However, with the increasing demand for BTX and the continuous petroleum consumption, the traditional petroleum refinery route to produce aromatics is difficult to meet the demands of the BTX market. In this context, the MTA conversion, as a petroleum-free route to obtain aromatics, would be a highly attractive alternative.^{11,13–15}

During the past decades, extensive attention has been attracted to this field, and a variety of zeolites have been explored as possible MTA catalysts. H-ZSM-5 is regarded as the most attractive

zeolite catalyst for the MTA conversion because of its suitable pore structure and adjustable acidic properties.^{16–18} As it is known, the MTH conversion over H-ZSM-5 zeolite follows a dual-cycle mechanism, i.e., olefin-based and aromatic-based cycles, which was first proposed by the Olsbye group.^{19,20} On the basis of this mechanism, we know that alkenes can simultaneously exist in H-ZSM-5 channels with aromatics as reaction intermediates and can also diffuse out of the pores as products. In this case, the selectivity to aromatics will be limited during the MTA conversion. Furthermore, the aromatics formed in the channels of H-ZSM-5 can further convert to polycyclic aromatic on the pore mouth or the external surface, which will rapidly deactivate the catalyst. To solve these problems of the MTA conversion on H-ZSM-5 catalysts, significant attention has been paid to improving the selectivity to aromatics and prolonging the catalyst lifetime.

Received: October 10, 2017

Revised: December 27, 2017

Published: January 3, 2018

For improving the selectivity to aromatics, modifying of H-ZSM-5 catalysts by metal species has been widely used, and the major active metal species used for the methanol aromatization are mainly Zn, Ga, La, Cu, Ag, and Ni.^{11–15,21–27} Especially, the Ga and Zn species are proved to be more active compared with other metal species, and the essential role of these active species originates from their dehydrogenation capability.^{11,28} Meanwhile, several strategies have been proposed to increase the catalyst stability during the MTH conversion. Modifying of the acid sites of the zeolites has been widely employed to suppress the catalyst deactivation, for instance, by adjusting the silicon content, isomorphous substitution of heteroatoms, and inactivating the acid sites on the external surface.^{29–36} Furthermore, synthesis of hierarchical ZSM-5 or mesoporous ZSM-5 and nano ZSM-5 zeolites has also been developed to improve their diffusion properties and to prolong the catalyst lifetime.^{11,13,37–44} Interestingly, recent studies from the Lercher group indicated that the cofeeding of olefins or higher alcohols with methanol resulted in a remarkable longer catalyst lifetime in MTO conversion because the high methylation rate competed with the formation of more deactivating coke compounds.⁴⁵ Until now, however, it has not been clarified whether this simple and efficient method to improve the catalyst stability can be extended to the MTA conversion. Also, if possible, it is the aim to investigate how the cofeeding reagents alter the dual-cycle mechanism during the MTA conversion. Especially, mechanistic investigations of the MTA conversion by sophisticated spectroscopic approaches are still missing up to now and are, therefore, the main goals of this work.

Taking all of the above-mentioned issues into consideration, in the present study, Ga-modified nano H-ZSM-5 catalysts with different Ga loadings of 1–5% have been prepared and used for MTA catalysts. Thereafter, the effects of Ga modification on the physicochemical properties and the catalytic performance of H-ZSM-5 catalysts during the MTA conversion were investigated. More importantly, the cofeeding of *n*-butanol with methanol in the MTA conversion was proved to be efficient in prolonging the catalyst lifetime. Additionally, the organic intermediates formed during the MTA conversion before and after *n*-butanol cofeeding were investigated via in situ UV/vis, TGA, GC–MS, and solid-state NMR spectroscopy. According to the catalytic and spectroscopic results, the reaction mechanism and the roles of *n*-butanol during the MTA conversion were elucidated.

2. EXPERIMENTAL SECTION

2.1. Preparation of the Materials. Nano H-ZSM-5 zeolite ($\text{SiO}_2/\text{Al}_2\text{O}_3 = 25$) was provided by Sinopec, China. The parent H-ZSM-5 material was impregnated with $(\text{Ga})_3\text{NO}_3$ aqueous solution and kept at 343 K for 12 h. Thereafter, the product was calcined at 873 K to derive Ga-modified H-ZSM-5 samples with different Ga loadings (1–5 wt %). The final products were labeled as *x*%-Ga-HZ-5, where *x* indicates the weight percent of the desired Ga loading and HZ-5 represents the H-ZSM-5.

2.2. Characterization of the Materials. X-ray diffraction (XRD) patterns of the parent and Ga-modified HZ-5 samples were recorded on a Bruker D8 diffractometer with $\text{CuK}\alpha$ radiation ($\lambda = 1.5418 \text{ \AA}$) at 5–50° and with a scan rate of $2\theta = 6.0^\circ/\text{min}$.

The surface areas and nitrogen adsorption isotherms of the prepared samples were measured by means of nitrogen adsorption at 77 K on a Quantachrome iQ-MP gas adsorption analyzer. Before the nitrogen adsorption, samples were dehydrated at 473 K for 2 h. The total surface area was calculated via the Brunauer–Emmett–Teller (BET) equation, and the micropore volume was determined using the t-plot method.

The chemical compositions of the prepared samples were determined by inductively coupled plasma emission spectrometry (ICP–AES) on a Thermo IRIS Intrepid II XSP atomic emission spectrometer.

TEM images of samples were acquired by a Philips Tecnai G2 F20 U-TWIN transmission electron microscope at an acceleration voltage of 200 kV. A few drops of alcohol suspension containing the samples were placed on a carbon-coated copper grid, followed by evaporation at ambient temperature.

Diffuse reflectance ultraviolet–visible (UV/vis) spectra of the zeolite samples were recorded in air against BaSO_4 in the region of 200–600 nm on a Varian Cary 300 UV–vis spectrophotometer.

NMR experiments were performed on a Bruker Avance III spectrometer at resonance frequencies of 400.1, 104.3, 79.5, and 122.0 MHz for ^1H , ^{27}Al , ^{29}Si , and ^{71}Ga nuclei, respectively. The experimental conditions are as follows: single pulse excitation of $\pi/2$ for ^1H and ^{29}Si , $\pi/6$ for ^{27}Al and ^{71}Ga , and repetition times of 20 s for ^1H and ^{29}Si and 0.5 s for ^{27}Al and ^{71}Ga MAS NMR spectroscopy. The ^1H , ^{27}Al , and ^{71}Ga MAS NMR spectra were recorded with a sample spinning rate of 8 kHz, while the ^{29}Si MAS NMR spectra were obtained with 4 kHz. The ^{27}Al , ^{29}Si , and ^{71}Ga MAS NMR measurements were performed with rehydrated samples. For this purpose, the samples were exposed to an atmosphere that was saturated with vapor of a $\text{Ca}(\text{NO}_3)_2$ solution at ambient temperature to be fully hydrated 1 day before the NMR investigations. Before the ^1H MAS NMR experiments, the samples were dehydrated at 723 K under a pressure below 10^{-2} Pa for 12 h. After dehydration, the samples were sealed and kept in glass tubes until they were filled into the MAS NMR rotors in a glovebox purged with dry nitrogen gas. The decomposition and simulation of the NMR spectra were carried out using the Bruker software WINNMR and WINFIT.

2.3. Catalytic Studies of the Zeolites under Study. The MTA conversion was investigated in a fixed-bed reactor at atmospheric pressure as reported in ref 33. Typically, 0.4 g of the catalysts (sieve fraction, 0.25–0.5 mm) were placed in a quartz reactor (5 mm i.d.) and activated under flowing helium gas at 723 K for 1 h. These samples were applied as MTA catalysts, at 723 K, and with a methanol flow corresponding to weight hourly space velocity (WHSV) of 1 h^{-1} . In the case of *n*-butanol cofeeding studies, the methanol and *n*-butanol flows were adjusted in such manner that equal total carbon numbers for all experiments were ensured. The hydrocarbon products were analyzed by an online gas chromatograph equipped with a flame ionization detector and a capillary column Plot Q to separate the reaction products, while the CO and CO_2 (together with CH_4) in the product were detected by TCD detector with a TDX-01 packed column, and CH_4 was used as a linkage for calibrating the concentrations of CO_x and hydrocarbons.

2.4. In Situ UV/Vis Studies of the Methanol Conversion on the 2%Ga-HZ-5 Catalysts. The nature of organic intermediates formed on the catalysts during the MTA conversion was in situ monitored by UV/vis spectroscopy as described in our previous work.³² The UV/vis spectra were recorded in the diffuse reflection mode in the range of 200–600 nm using an AvaSpec-2048 fiber optic spectrometer, an AvaLight-DH-S light source by Avantes, and a glass fiber reflection probe FCR-7UV200C-2-BX-HTX. Before the MTA conversion was started, the glass fiber reflection probe was placed in the fixed-bed reactor on the top of the catalyst bed with a gap of ca. 1.0 mm. Reference UV/vis spectra of the fresh catalysts were recorded at reaction temperature prior to starting the methanol flow.

2.5. TGA and GC–MS Analysis of Organic Deposits on the Used 4%Ga–HZ-5 Catalysts. The amounts of organic deposits on the used 4%Ga–HZ-5 catalysts after the MTA conversion, performed with different time-on-stream (TOS), were analyzed by thermogravimetric analysis (TGA) on a Setram Setsys 16/18 thermogravimetric analyzer. In a typical measurement, 0.1 g of the used catalyst material was heated in an Al₂O₃ crucible with a constant heating rate of 10 K/min and under flowing (30 mL/min) synthetic air.

The nature of the organic deposits on the catalysts after the MTA conversion at different TOS was analyzed by gas chromatography–mass spectrometry (GC–MS). Typically, 0.1 g of the used catalyst was carefully dissolved in 1 M HF solution. This solution was treated with CH₂Cl₂ to extract the organic compounds, and the residual water was removed by addition of sufficient sodium sulfate. Then, 0.2 μ L of the organic extract was analyzed by GC–MS (GCMS-QP2010 SE) with a RXI-5MS column (length of 30 m, 0.25 mm i.d., stationary phase thickness 0.25 μ m). The following temperature program was employed: Isothermal heating at 313 K for 6 min, heating to 553 K with a rate of 10 K/min, and isothermal heating at 553 K for 10 min.

2.6. Computational Methods and Modeling. All periodic DFT calculations were carried out using the VASP Package. The Bayesian error estimation functional with vdW correlation (BEEF-vdW) was employed. The electron–ion interaction was described by the projector augmented wave (PAW) method. The plane wave basis set kinetic energy cutoff was 400 eV. The sampling of Brillouin zone was only with Γ point. The dimer method was utilized to locate transition states. A force threshold of 0.01 eV/Å was used for structure optimization of all intermediates and transition states. The frequency calculations employed a partial Hessian approach, including the H atoms of acid sites and organic species part of involved states. The enthalpies, entropies, and free energies of the reaction cycles at 723 K were calculated from harmonic frequencies.^{46–49}

The HZ-5 was modeled by a periodic orthorhombic cell consisting of 96 T atoms. The framework aluminum atom was situated at a T12 site of the ZSM-5 cell. The lattice constants were optimized as $a = 20.36$ Å, $b = 20.05$ Å, $c = 13.48$ Å. All atoms in the cell were allowed to relax with the lattice constants being fixed.⁵⁰

3. RESULTS AND DISCUSSION

3.1. Physicochemical Properties of the Catalyst Materials. The XRD patterns of parent and Ga-modified HZ-5 samples are shown in Figure S1. For the parent HZ-5 catalyst, typical diffraction lines corresponding to a MFI structure were observed, indicating that a pure phase was obtained.⁵¹ After Ga modification, similar diffraction patterns with only a slight decrease of the relative crystallinity as those of parent HZ-5 could be observed for all the Ga-modified HZ-5 samples, indicating the primary MFI structure is well preserved upon the Ga modification. Additionally, no XRD reflections due to bulk Ga₂O₃ phase were observed from the XRD patterns of Ga-modified HZ-5, indicating the Ga species of the modified HZ-5 samples were highly dispersed in zeolite pores.

For a better understanding of the effects of Ga modification on the textual properties of HZ-5 samples, multinuclear solid-state NMR spectroscopy was employed. Figure S2 shows the ²⁷Al and ²⁹Si MAS NMR spectra of the parent and Ga-modified HZ-5 materials. For all ²⁷Al MAS NMR spectra, the dominant signals at 56 ppm are due to tetrahedral aluminum atoms, and the weak signals at 0 ppm are caused by octahedrally coordinated aluminum species.⁵² With the introduction of Ga into the parent HZ-5

samples, no changes of the signal intensities and no occurrence of additional signals could be observed, indicating the HZ-5 framework is well preserved. These observations were also supported by the ²⁹Si MAS NMR spectra in Figure S2, right, which consist of signals between –107 and –116 ppm. These signals are due to silicon atoms at crystallographic Si(1Al, 3Si) and Si(4Si) sites, respectively, which are also not changed after Ga impregnation.⁵³

The hydroxyl groups in the parent and Ga-modified HZ-5 materials were analyzed by ¹H MAS NMR spectroscopy. As shown in Figure 1, two strong signals at 1.3 and 3.6 ppm occur in

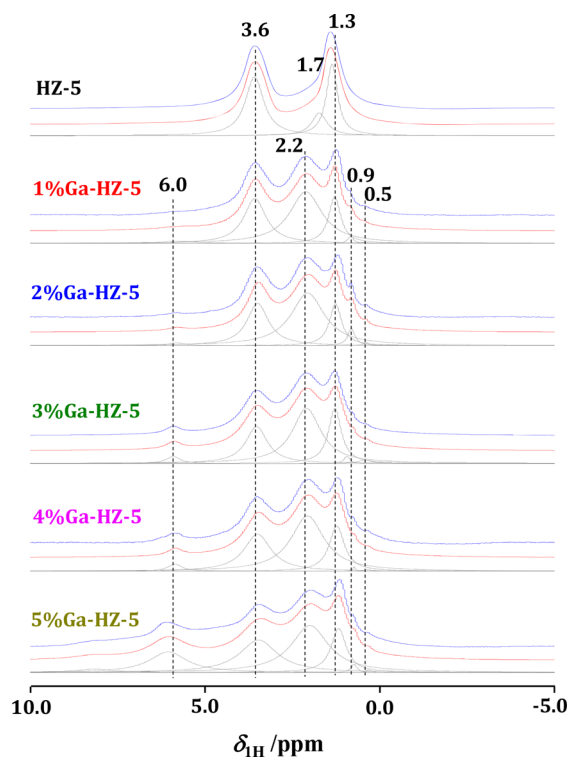


Figure 1. ¹H MAS NMR spectra of the parent and Ga-modified HZ-5 zeolites.

the spectrum of the parent HZ-5, which are due to silanol groups at framework defects and acidic bridging hydroxyl groups (Si(OH)Al), i.e., Brønsted acid sites, respectively.⁵⁴ The weak signal shoulder at 1.7 ppm can be also ascribed to silanol groups at different framework defects. After Ga impregnation, a strong new signal at 2.2 ppm and several weak signals at 0.5, 0.9, and 6.0 ppm appear. The new signals at 0.5–0.9 ppm are attributed to Ga–OH groups at the outer particle surface, while the signals at 2.2 and 6.0 ppm indicate the presence of Ga–OH groups involved in hydrogen bonding, probably inside the HZ-5 pores, as also observed for La–OH groups in zeolite Y.^{52,55,56} The quantitative analysis of the Brønsted acid sites of the samples is summarized in Table 1 (column 6). Obviously, Ga introduction causes a strong decrease of Brønsted acid site density of the modified HZ-5 samples. Typically, the concentration of Brønsted acid sites decreases from 0.32 mmol/g in parent HZ-5 to 0.16 mmol/g in 5%Ga–HZ-5 (Table 1), probably due to cationic Ga species replacing hydroxyl protons of former Si(OH)Al groups.

Figure S3 shows the representative TEM image of the 4%Ga–HZ-5 catalyst. In this image, no clusters of Ga species can be observed. However, the EDX measurements, which are also shown in Figure S3, reveal that the Ga was indeed present in the sample. These findings indicate the presence of well-dispersed

Table 1. Chemical Composition and Surface Area of the Parent and Ga-Modified HZ-5 Samples under Study

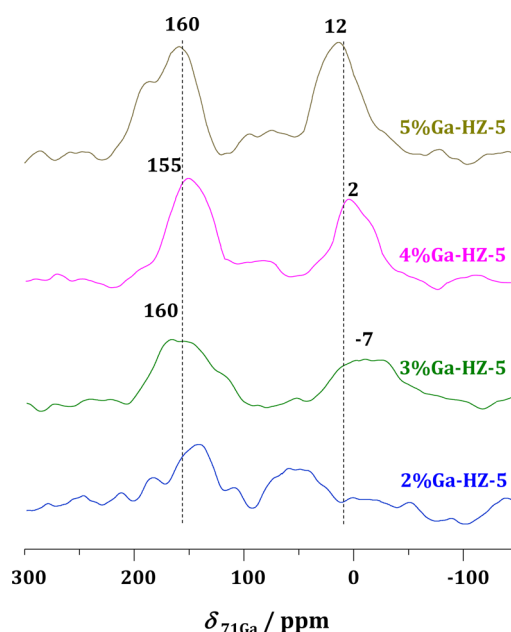
samples	Si/Al ^a	Ga loading (wt %)	S _{BET} ^b (m ² /g)	V _{micro} ^c (cm ³ /g)	n _{Si(OH)Al} ^d (mmol/g)
HZ-5	12.5	–	451	0.28	0.32
1%Ga-HZ-5	12.3	0.9	446	0.27	0.29
2%Ga-HZ-5	12.6	1.9	438	0.27	0.26
3%Ga-HZ-5	12.8	2.8	430	0.26	0.24
4%Ga-HZ-5	13.1	3.8	426	0.25	0.21
5%Ga-HZ-5	14.2	4.7	418	0.24	0.16

^aDetermined by ICP-AES. ^bDetermined by N₂-absorption. ^cMicropore volume was estimated by using the t-plot method. ^dDetermined by ¹H MAS NMR.

Ga species in the HZ-5 pores, which is in accordance with the XRD results. In Table 1, the textural properties of the Ga-modified HZ-5 samples under study are summarized. These data indicate that no significant changes of the surface areas and micropore volumes occurred after the Ga impregnation. This implies that Ga introduction does not influence the characteristics of the HZ-5 sample under study.

Direct investigations of the nature of Ga species in the Ga-modified HZ-5 catalysts were performed by UV/vis and ⁷¹Ga MAS NMR spectroscopy. As shown in the UV/vis spectra in Figure S4, all the Ga-containing catalysts exhibit similar adsorption bands at about 215 and 280 nm. The former band is attributed to the charge transfer transition of gallium species coordinated with O²⁻ species, which is characteristic of isolated tetrahedrally coordinated Ga atoms. The band at about 280 nm could be ascribed to isolated extra-framework Ga species.⁵⁷ The intensities of these bands greatly develop with the increase of Ga contents. Moreover, no absorption bands at about more than 350 nm appear in the spectra of Ga-modified HZ-5 catalysts, indicating that no bulk Ga₂O₃ particles were formed.⁵⁸ This result is well in accordance with the XRD (Figure S1) and TEM (Figure S3) results, in which no signs of bulk Ga₂O₃ formation can be detected. The ⁷¹Ga MAS NMR spectra of the Ga-modified HZ-5 samples are shown in Figure 2. For all the samples, very broad signals of tetrahedrally coordinated Ga species at 150–160 ppm and octahedrally coordinated Ga species at –7 to 12 ppm occur.^{59–61} The strong broadening of these signals indicates that they are due to oxidic extra-framework Ga species or extra-framework Ga cations with a corresponding oxygen coordination. In contrast, tetrahedrally coordinated framework Ga species give more narrow ⁷¹Ga MAS NMR signals at 150 ppm due to their well-defined local structure.⁵⁹ Hence, the ⁷¹Ga MAS NMR spectra in Figure 2 hint at the formation of different extra-framework Ga species, such as Ga³⁺, GaO(OH), and highly dispersed Ga₂O₃, inside the pores of the Ga-modified HZ-5 samples, which agrees well with the findings from other spectroscopic methods.

3.2. Catalytic Performance of the Parent and Ga-Modified HZ-5 Catalysts in the MTA Conversion. According to previous studies, Zn or Ga modification of HZ-5 can significantly increase the selectivity to aromatics in MTA conversion.²⁸ In order to compare the effect of Ga modification on the catalytic performance of HZ-5 in MTA conversion, the time dependence of the methanol conversion and the selectivity to aromatics on the parent and Ga-modified HZ-5 catalysts are shown in Figure 3. It is clear that the Ga modification has a strong impact on the catalyst lifetime during the MTA conversion (Figure 3a). For the parent HZ-5 catalyst, the catalyst lifetime with a methanol conversion >99% can be maintained up to 30 h. For Ga-modified

**Figure 2.** ⁷¹Ga MAS NMR spectra of the Ga-modified HZ-5 zeolites.

HZ-5 catalysts, the catalyst lifetime gradually decreases with the increase of gallium contents and can drop down to 15 h on the 5%Ga-HZ-5 catalyst. On the other hand, as shown in Figure 3b, the selectivity to aromatics increased from 28% for the parent HZ-5 zeolite to 49.3% for the 1%Ga-HZ-5 catalyst. The ¹H and ⁷¹Ga MAS NMR results indicate that different extra-framework Ga species, such as Ga³⁺, GaO(OH), and highly dispersed Ga₂O₃, can be formed on HZ-5 after the Ga introduction, and the cationic Ga species can replace the hydroxyl protons of Si(OH)Al groups and lead to decrease of the concentration of Brønsted acid sites (Table 1, column 6). According to the previous study of Narula and co-workers,⁶² the exchanged Ga sites are responsible for the increased aromatics production. Therefore, with the further increase of the Ga content, the selectivity to aromatics increased up to 66.7% for the 5%Ga-HZ-5 catalyst. On the other hand, according to our previous studies, the decrease of Brønsted acid sites in zeolite catalysts could prolong the catalyst lifetime during the methanol conversion.³³ Therefore, the rapid deactivation of the Ga-modified HZ-5 catalysts under study should be explained from other aspects. Based on the dual-cycle mechanism of MTH conversion, the role of Ga species during the MTA conversion is promoting the olefin cycle to aromatics cycle (Scheme S1), accompanied by rapid accumulation of coke deposits, which is similar to the former reports for the role of Ga in ethanol to aromatics conversion.⁶² The enhanced coke formation is supported by the TGA results (Figure S5), since significantly higher coke contents (9.5%) on the used 4%Ga-HZ-5 than on the parent HZ-5 (7.6%) were observed after a MTA conversion at TOS = 10 h under same reaction conditions. The higher selectivity to aromatics of the HZ-5 catalysts with high Ga contents is accompanied by an enhanced coke formation and catalyst deactivation. Therefore, methods are required that help to suppress the coke formation on highly selective MTA catalysts. In the further studies, the 4% Ga-HZ-5 catalyst with a similar catalytic performance to 5%Ga-HZ-5 was utilized as the model catalyst.

3.3. Effect of *n*-Butanol Cofeeding on the Catalytic Performance of the 4%Ga-HZ-5 Catalyst during the MTA Conversion. According to previous studies, cofeeding of small contents of higher alcohols can strongly increase the catalyst

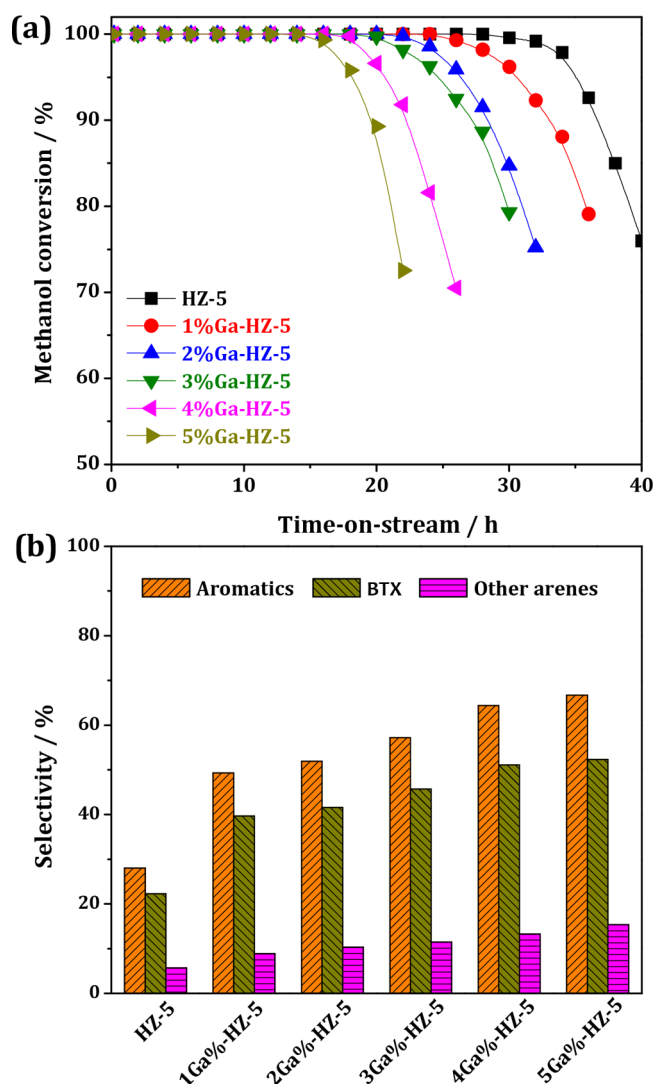


Figure 3. (a) Methanol conversion variation with time-on-stream over the parent and Ga-modified HZ-5 zeolites. (b) The selectivity of total aromatics, BTX, and other arenes over the parent and Ga-modified HZ-5 zeolites at 723 K and with a TOS of 2 h.

lifetime during the MTH conversion.⁴⁵ Therefore, for increasing the stability of the 4%Ga-HZ-5 catalyst during the MTA conversion under study, different amounts of *n*-butanol were cofed with methanol, and the time dependencies of the catalytic performance on 4%Ga-HZ-5 catalyst with and without *n*-butanol cofeeding are shown in Figure 4. For the MTA conversion without *n*-butanol cofeeding, a rapid deactivation occurs: the catalyst lifetime with a methanol conversion >99% is only about 18 h. With *n*-butanol cofeeding, however, a significant prolongation of the catalyst lifetime with more than 40 h was obtained, and the main difference in the product distributions was the selectivity to larger aromatics, while the total yield of aromatics remained stable (Table S1). Additionally, with the gradual increase of the *n*-butanol ratio from 10% to 50% in the feed, 100% methanol and *n*-butanol conversion can be obtained. Meanwhile, the selectivity to aromatics gradually decreased, while the selectivity to olefins gradually increased simultaneously. According to the calculation results (vide infra, Section 3.8), the cofed *n*-butanol preferentially adsorbs at the acid sites of the HZ-5 catalysts and further transfers to *n*-butene. Some of the formed *n*-butene can diffuse out of the pores of the ZSM-5 catalyst as products, which leads to an

increase of the selectivity to butene (Table S1). On the other side, the inescapable *n*-butene can directly participate in the olefin-based cycle via the reaction with methanol, which can suppress the aromatic-based cycle and lead the decrease of the selectivity to larger aromatics, i.e., C₉⁺ aromatics (Table S1). In addition, with the progress of the MTA conversion, the gradual decrease of the selectivity to aromatics can be observed both before and after the *n*-butanol cofeeding, which is due to the gradual coverage of the Ga species being active in aromatization reactions. The formation of coke compounds on these Ga species was supported by the ⁷¹Ga MAS NMR spectra (vide infra). Interestingly, under the optimum ratio of methanol and *n*-butanol, i.e., 85% methanol and 15% *n*-butanol, a stable activity with the selectivity to aromatics of 45–60% could be achieved up to TOS = 40 h, and a longer catalytic lifetime with a methanol conversion >99% could be obtained up to TOS = 50 h (Figure S6).

Under the same reaction conditions, the regenerability of the used 4%Ga-HZ-5 was investigated by calcination in air at 873 K for 4 h. The reaction time dependence of the MTA conversion of the regenerated 4%Ga-HZ-5 catalyst is shown in Figure S6. The stable activity for a methanol conversion >99% could be near fully recovered after regeneration. This indicates that carbon deposits are responsible for the catalyst deactivation. In addition, we also investigated the effect of ethanol and propanol cofeeding with methanol on the catalytic performance of MTA conversion and found that ethanol cofeeding had nearly no influence on the catalytic performance. However, propanol cofeeding could slightly increase the catalyst lifetime but not as strong as that of butanol (Table S2). Interestingly, after ethanol or propanol cofeeding, the selectivity to ethene or propene greatly increased, which indicates that the main contents of the formed ethene or propene could directly diffuse out of the pores of ZSM-5 catalysts as products but are not involved in the next reaction, and therefore, the dual-cycle mechanism was not well altered.

3.4. TGA and GC-MS Analysis of Organic Deposits on the Used 4%Ga-HZ-5 Catalysts. To quantify the organic deposits formed on 4%Ga-HZ-5 after MTA conversion for different TOS = 1.0–40 h, the weight losses in the temperature range of 298–1073 K were determined by TGA. According to Figure 5, two obvious weight losses can be recognized: a low-temperature weight loss at 573 K and a high-temperature weight loss at >573 K, which are ascribed to desorption of water and coke compounds, respectively.⁶³ In the high-temperature range of 573–1073 K, similar variation tendency of weight losses could be observed for the used catalysts after the MTA conversion with and without *n*-butanol cofeeding. However, the weight losses of the used catalysts after the pure methanol conversion are higher than those of the methanol/*n*-butanol mixture conversion at the same TOS. For the pure methanol conversion, the weight losses of the catalysts increased from 5.9% to 20.4% with the progress of the reaction time from TOS = 1.0–40 h, while the weight losses of the catalysts obtained with the methanol/*n*-butanol mixture conversion increased from 4.1% to 16.4% for the same reaction times and conditions. To compare the coke formation during the conversion of the above-mentioned two different feeds more directly, the average coke formation rate (R_{coke}) and the fraction of methanol consumed for coke formation (W_{coke}) were also evaluated and are given in Table 2, columns 3 and 4, respectively. It is obvious that the accumulation of organic compounds on 4%Ga-HZ-5 catalysts during the MTA conversion is suppressed by the *n*-butanol cofeeding.

The chemical composition of the organic compounds occluded in the catalysts obtained after MTA conversion with different TOS of 1.0–40 h was analyzed by GC-MS, and the results are

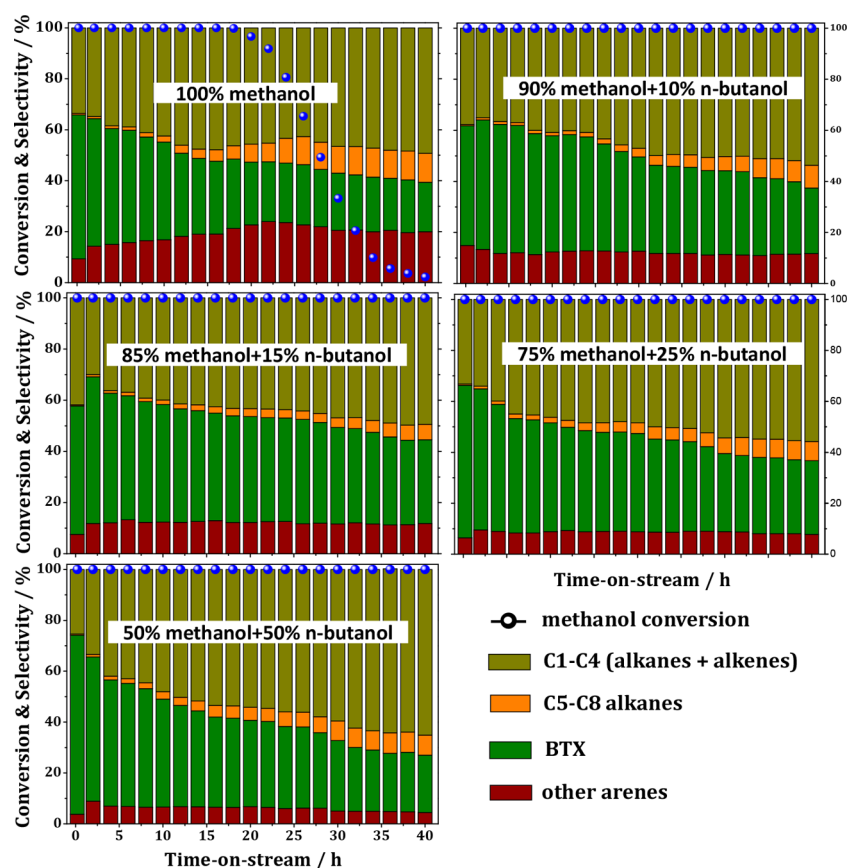


Figure 4. Methanol conversion and hydrocarbon product distribution over 4%Ga-HZ-5 catalysts at 723 K and with a TOS of 40 h using methanol or a mixture of methanol and *n*-butanol as reagents. The concentrations of methanol in the methanol and *n*-butanol mixture shown in the figures are in the ranges of 100–50%. (100% *n*-butanol conversions with a TOS of 40 h can be obtained in all the *n*-butanol cofeeding experiments, which are not shown here).

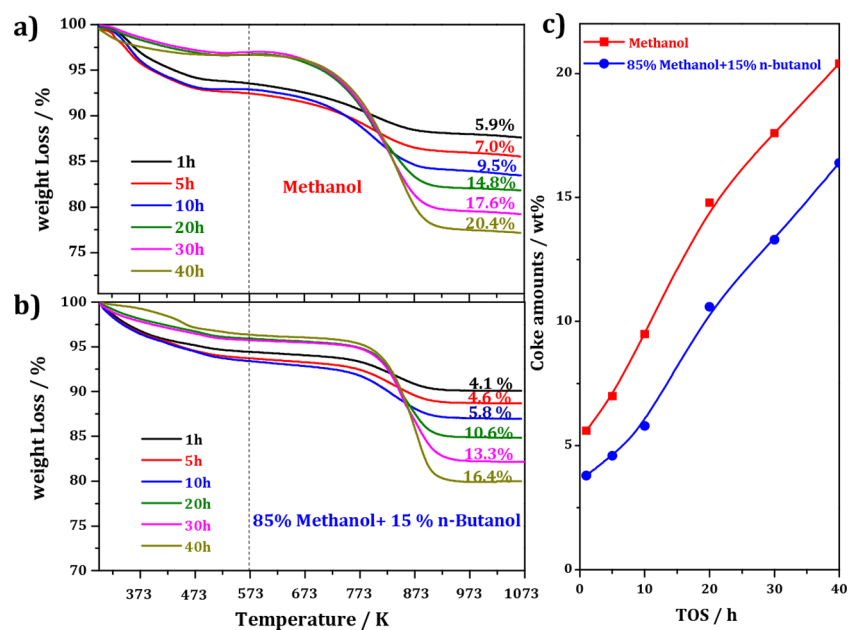


Figure 5. TGA curves of spent 4%Ga-HZ-5 catalysts obtained after MTA conversion at 723 K with different TOS. (a) Methanol conversion. (b) Conversion of 85% methanol and cofeeding of 15% *n*-butanol. (c) Direct comparison of the coke amounts over 4%Ga-HZ-5 catalysts with the different TOS before and after *n*-butanol cofeeding.

shown in Figure 6. Mainly, polymethylaromatics with one to three condensed aromatic rings were detected for all used catalysts. The concentrations and proportions of these organic deposits, reflected as the intensities of the GC–MS signals, changed

significantly with increasing TOS. Typically, naphthalene and anthracene are the dominant deposits formed on the used catalyst samples, even within the short TOS of 5.0 h during the MTA conversion. In contrast, for the used catalysts obtained after MTA

Table 2. Coke Amount, Average Coke Formation rate (R_{coke}), and Fraction of the Methanol Consumption for Coke Formation (W_{coke}) during the MTA Conversion with and without *n*-Butanol Cofeeding over Ga-ZSM-5 Catalysts under Study, Determined for TOS = 40 h

reagent	coke (wt %)	R_{coke} (mg/min)	W_{coke} (g/g)
methanol	20.4	0.034	0.007
85% methanol + 15% <i>n</i> -butanol	16.4	0.027	0.004

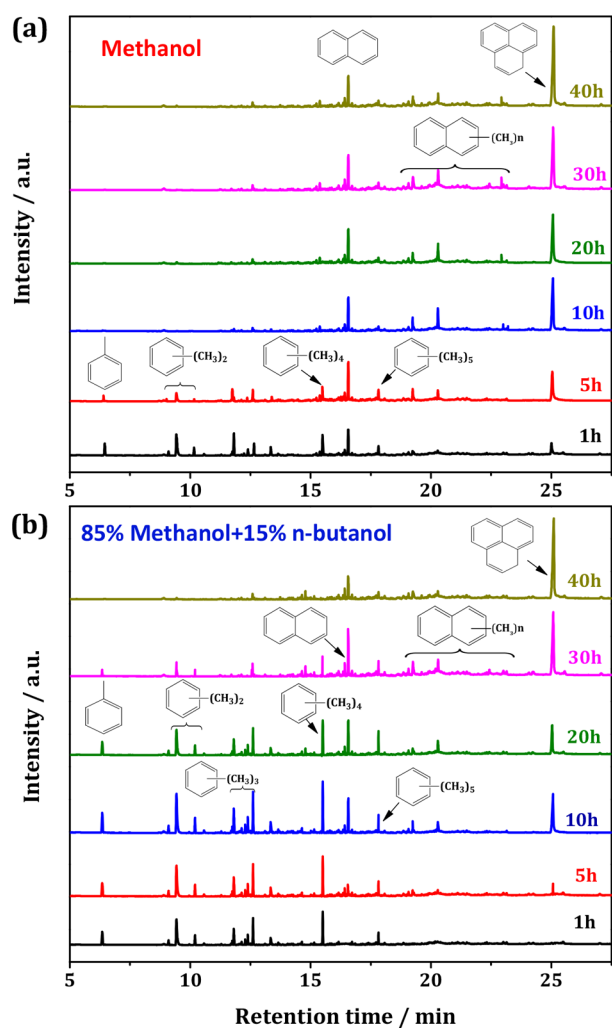


Figure 6. GC-MS chromatograms of the organic extracts from 4%Ga-HZ-5 catalysts obtained after MTA conversion at 723 K with different TOS. (a) Methanol conversion. (b) Conversion of 85% methanol and cofeeding of 15% *n*-butanol.

conversion with cofeeding of *n*-butanol, polymethylbenzenes were observed as major organic species on the used catalyst samples obtained up to TOS = 20 h, and thereafter naphthalene and anthracene become the dominant species. On the basis of these observations, it can be concluded that the accumulation of larger organic compounds, like naphthalene and anthracene, could be strongly postponed after cofeeding with *n*-butanol during the MTA conversion, which also agrees with the TGA results. Therefore, longer catalyst lifetimes could be achieved with *n*-butanol cofeeding during the MTA conversion.

3.5. In Situ UV/Vis Studies of Intermediates Formed during the MTA Conversion over 4%Ga-HZ-5 Catalysts. The amounts and chemical compositions of organic deposits on

the used catalysts were obtained by the above-mentioned TGA and GC-MS studies, while the detailed information on the nature of these organic compounds formed during the MTA conversion with and without *n*-butanol cofeeding was more challenging. Therefore, in situ UV/vis spectroscopy was utilized to investigate the nature of the organic deposits on the used catalysts. In Figure 7,

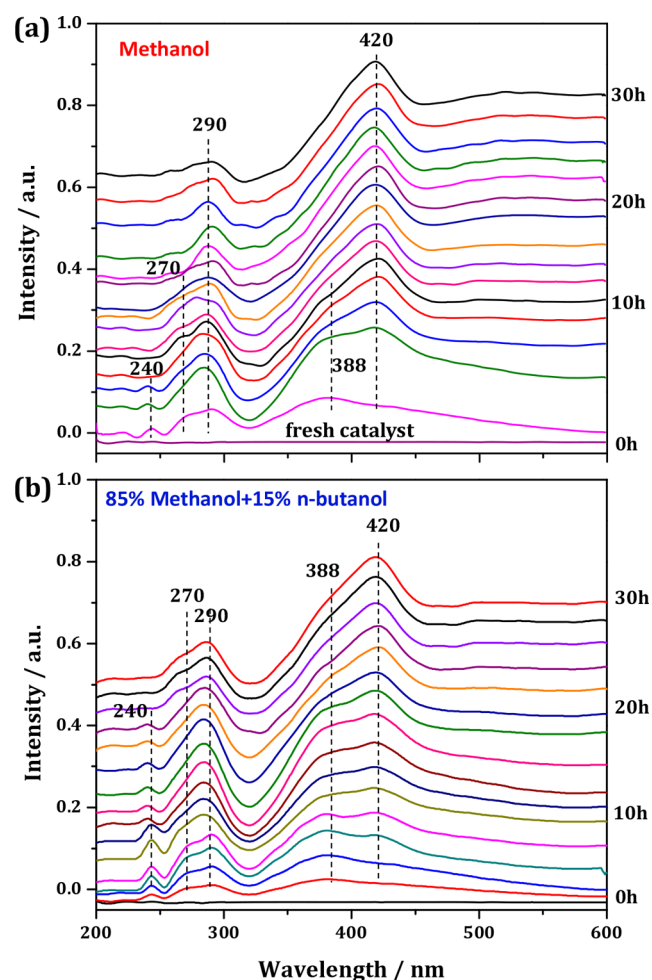


Figure 7. In situ UV/vis spectra recorded during the MTA conversion over 4%Ga-HZ-5 catalysts at 723 K and up to TOS = 30 h. (a) Methanol conversion. (b) Conversion of 85% methanol and cofeeding of 15% *n*-butanol.

the in situ UV/vis spectra recorded during the MTA conversion without and with *n*-butanol cofeeding over the 4%Ga-HZ-5 catalyst at 723 K up to TOS = 30 h are shown. Comparing the methanol conversion without and with *n*-butanol cofeeding, similar organic species were formed during the MTA conversion as indicated by UV/vis bands at 240, 270–290, and 388–420 nm. According to the previous studies,^{64,65} the band at 240 nm was attributed to dienes, while the bands at 270–290 nm are assigned to monoenylic carbenium ions or polyalkylaromatics species. Bands at 388–420 nm hint to the formation of dienylic carbenium ions and polycyclic aromatics. The latter species formed with two or three condensed aromatic rings occur at wavelengths lower than 400 nm, while those formed with four condensed aromatic rings occur at wavelengths slightly higher than 400 nm.⁶⁵ The concentrations of all organic species, reflected as the intensities of corresponding UV/vis bands, change distinctly with the progress of the MTA conversion. The bands of dienes (240 nm) gradually disappeared, while the bands of

monoenylic carbenium ions or polyalkylbenzenes (270–290 nm) gradually increased. Simultaneously, benzene-based carbenium ions (~388 nm) are gradually transferred to polycyclic aromatics (~400 nm). These observations indicate that monoenylic carbenium ions or polyalkylaromatics species are formed from dienes, while the polycyclic aromatics are formed from the benzene-based carbenium ions. Additionally, the in situ UV/vis spectra also reveal that the accumulation of polycyclic aromatics is strongly decreased with *n*-butanol cofeeding during the MTA conversion, which agrees well with the TGA and GC–MS results.

In order to get more formation about the organic species formed during the early stages of the MTA conversion, a direct comparison of the UV/vis spectra recorded at TOS = 5 min during the MTA conversion with and without *n*-butanol cofeeding are given in Figure 8. Obviously, a very rapid formation of

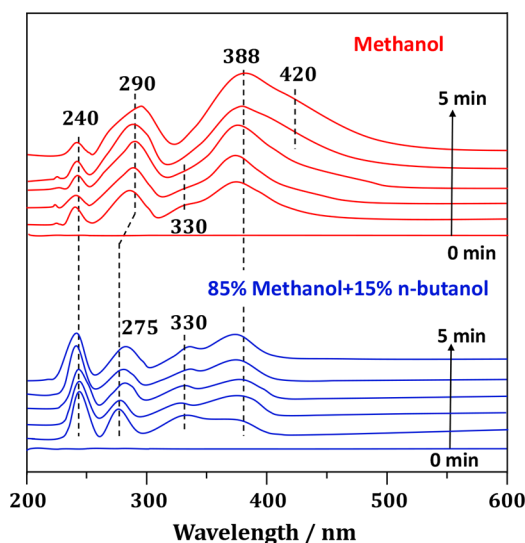


Figure 8. In situ UV/vis spectra recorded during the initial process of MTA conversion over 4%Ga-HZ-5 catalysts at 723 K with a TOS = 5 min. (Red line) Methanol conversion. (Blue line) Conversion of 85% methanol and cofeeding of 15% *n*-butanol.

polyalkylbenzenes (~290 nm) and polycyclic aromatics (~400 nm) can be observed during the first minute of the pure methanol conversion (Figure 8, top). For cofeeding with *n*-butanol (Figure 8, bottom), the bands of polyalkylbenzenes (290 nm) have a blue shift to about 275 nm, indicating that carbon chain growth or cyclization reactions are suppressed. Simultaneously, the formation of polycyclic aromatics is strongly decreased, and dienes are observed as the dominant organic compounds. According to our previous studies,³³ these dienes are formed from long-chain alkenes according the olefin-based cycle mechanism and can also act as the catalytically active hydrocarbons during the methanol conversion. Additionally, new signals at 330 nm due to dienyl carbenium ion also occur in the UV/vis spectra, which can be gradually transformed to benzene-based carbenium ions (~388 nm) and trienylic carbenium ions/polycyclic aromatics (~420 nm). These observations indicate that the dual-cycle mechanism during the MTA conversion can be altered via the cofeeding of *n*-butanol, i.e., the proportion of the olefin-based cycle is promoted by the cofeeding of *n*-butanol (vide infra). Therefore, the accumulation of polycyclic aromatics is strongly suppressed, and longer catalyst lifetimes can be achieved in this way.

3.6. ⁷¹Ga MAS NMR Studies of the Ga Species in the Fresh, Deactivated, and Regenerated 4%Ga-HZ-5 Catalysts. To get more information about the effects of coke compounds

on the existence states of Ga species in the 4%Ga-HZ-5 model catalysts after the MTA conversion, ⁷¹Ga MAS NMR characterizations were performed. For the 4%Ga-HZ-5 catalyst obtained after MTA conversion with cofeeding of *n*-butanol at TOS = 40 h, a strong decrease of the ⁷¹Ga MAS NMR signals occurs (Figures 9a

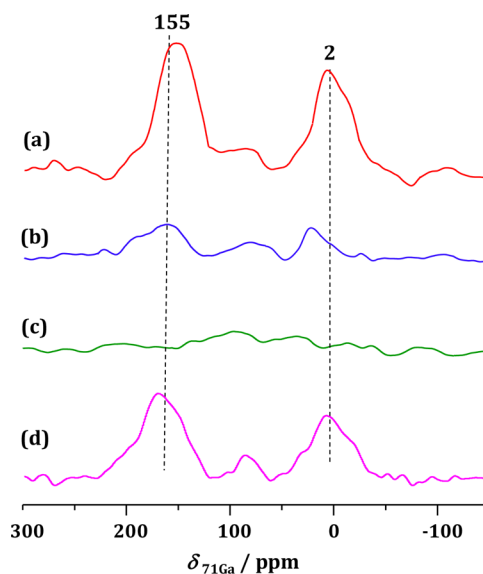


Figure 9. ⁷¹Ga MAS NMR spectra of the fresh 4%Ga-HZ-5 catalyst (a), the used 4%Ga-HZ-5 catalysts obtained after MTA conversion with (b) and without (c) *n*-butanol cofeeding at a TOS of 40 h, and the regenerated (d) 4%Ga-HZ-5 catalyst from (c).

and 9b), which indicates the coverage of the Ga species by coke compounds. In this case, the Ga species cannot be fully hydrated before the ⁷¹Ga MAS NMR measurements, which leads to a strong increase of the quadrupolar interactions (⁷¹Ga: spin *I* = 3/2) and a corresponding strong line broadening.⁵⁹ In contrast, nearly no signals can be observed in the ⁷¹Ga MAS NMR spectrum for the totally deactivated 4%Ga-HZ-5 obtained after MTA conversion at TOS = 40 h (Figure 9c). This indicates a complete coverage of the gallium species by coke compounds on the deactivated catalyst, which makes the Ga species nonaccessible for water molecules. After regeneration of the deactivated 4%Ga-HZ-5, however, similar ⁷¹Ga MAS NMR signals with intensities comparable to those of the nonused 4%Ga-HZ-5 sample are observed in the ⁷¹Ga MAS NMR spectra (Figures 9a and 9d). These observations indicate that the accumulation of large polycyclic aromatics is the reason for a catalyst deactivation due to pore blocking or a complete coverage of the active sites making them nonaccessible for further reactants. In addition, the ⁷¹Ga MAS NMR signal intensities of the regenerated catalyst cannot be fully recovered in comparison with the fresh sample (Figure 9), which can be due to the incomplete removal of the coke compounds, as the regeneration of the deactivated catalyst was performed in flowing air at 873 K for 4 h. According to the TGA results in Figure 5, the coke compounds formed during the MTA conversion could not be totally decomposed at 873 K. Therefore, the ⁷¹Ga MAS NMR signal intensities of the Ga-modified HZ-5 catalyst could not be completely recovered after the regeneration, which is also supported by the incomplete recovery of the catalyst lifetime in the generated catalyst (Figure S6).

3.7. Deactivation Mechanism of MTA Reaction over 4%Ga-HZ-5 Catalysts. Several complementary approaches, e.g., TGA, GC–MS, in situ UV/vis, and ⁷¹Ga MAS NMR spectroscopy,

can give detailed insights into the reaction and deactivation mechanism of MTA conversion over Ga-modified HZ-5 catalysts.

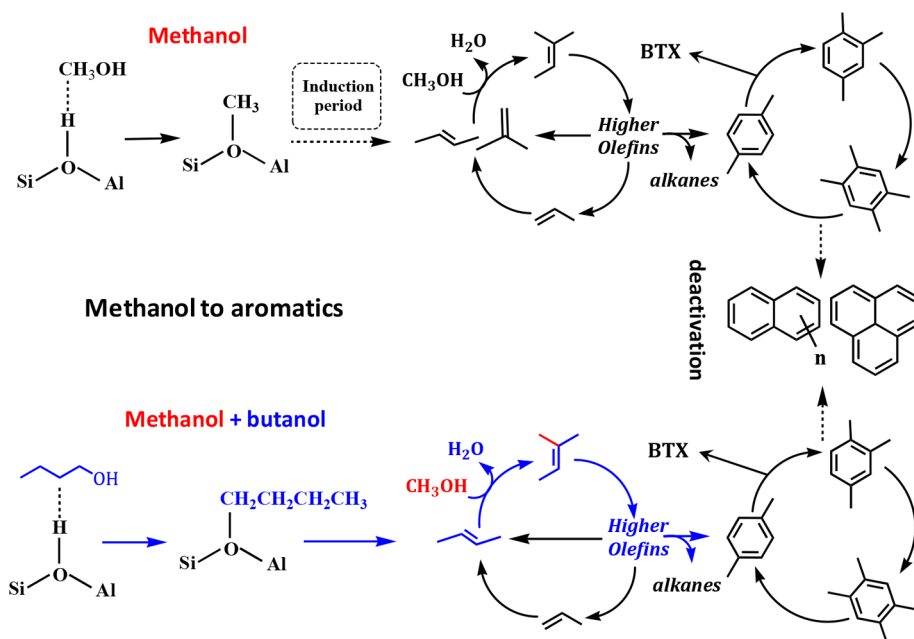
As demonstrated by in situ UV/vis spectroscopy (Figure 7), similar organic intermediates and their variation tendencies are observed during the MTA conversion with and without *n*-butanol cofeeding. Dienes (240 nm), as the dominant intermediates during the early stages of the MTA conversion, can rapidly convert to monoenylic carbenium ions or polymethylbenzenes (270–290 nm) and, then, to dienylic carbenium ions (330 nm). With further progress of the MTA conversion, the dienylic carbenium ions are gradually transferred to benzene-based carbenium ions (~388 nm), and a transformation of benzene-based carbenium ions to trienylic carbenium ions/polycyclic aromatics (~420 nm) occurs, which is also supported by the GC–MS results (Figure 6). Generally, the formation of the small polycyclic aromatics can cause a rapid deactivation of catalysts with chabasite (CHA) cages, like SAPO-34.⁶⁴ Interestingly, the Ga-modified HZ-5 catalysts under study still exhibit a high activity (Figure 4), when polycyclic aromatics become the dominant organic species after TOS = 10 h (Figure 6 and 7), and the activity is stable up to TOS = 25 h. It means that polycyclic aromatics (maximum two condensed aromatic rings), e.g., polyalkylnaphthalene- or naphthalene-based carbenium ions, can also serve as active intermediates, which supports the recent studies of Liu et al.⁶⁶ However, with further progress of the MTA conversion, a surplus of these aromatic species in the H-ZSM-5 channels is transferred to much larger polycyclic aromatics, i.e., three to four condensed aromatic rings, as indicated by the UV/vis and GC–MS results (Scheme 1, red frame). Finally, these large polycyclic aromatics cause a total blocking of the HZ-5 channels, which strongly hinders the diffusion of reaction products and makes all catalytically active sites nonaccessible for further reactants. This is also supported by the nonhydrated gallium species in the used catalysts and the rehydrated gallium species in the generated catalysts (Figure 9).

3.8. Mechanistic Interpretation of the Enhanced Catalyst Lifetime by *n*-Butanol Cofeeding during the MTA Conversion. The deactivation mechanism of the Ga-modified

HZ-5 catalysts during the MTA conversion is elucidated as mentioned above, while the roles of *n*-butanol in the enhancement of the catalyst lifetime are still not clear and are, therefore, focused on in the present work. According to the previous studies, alkenes formed during the induction period of the MTO conversion can act as the initial active species for the propagation of higher alkene chains.^{33,67} Subsequently, the long-chain alkenes can act as active hydrocarbon species and be cracked to lower olefins according to the olefin-based cycle mechanism. Simultaneously, long-chain alkenes can be further methylated and converted to dienes, which are also active hydrocarbon species. The above-mentioned dienes cause the UV/vis band at about 240 nm occurring in Figure 8. Generally, this reaction period is short, and dienes can be immediately converted to other larger intermediates, e.g., polymethylbenzenes and dienylic carbenium ions. Thereafter, the aromatic-based cycle together with the olefin-based cycle of the dual-cycle mechanism starts to contribute to the methanol conversion (Scheme 1, red frame).

Here, the first step of methanol conversion, i.e., the formation of methoxy species upon adsorption of methanol molecule onto the Brønsted acid sites of the HZ-5 catalyst, is competed by the cofeeding *n*-butanol. The adsorption enthalpies of methanol and *n*-butanol, calculated via DFT methods using a periodic H-ZSM-5 cell, are –102 and –128 kJ/mol, respectively (Figure 10). Therefore, *n*-butanol will preferentially adsorb at the acid site of H-ZSM-5 catalysts during its cofeeding. At 0 K, the dissociative enthalpy barrier for the transformation of *n*-butanol into *n*-butoxide is 90 kJ/mol, much lower than that for the transformation of methanol into methoxide (128 kJ/mol). At the reaction temperature of 723 K, the Gibbs free energy barriers are 114 and 137 kJ/mol for the dissociation of *n*-butanol and methanol, respectively. Therefore, after the cofeeding of *n*-butanol with methanol, *n*-butanol is preferentially transformed into *n*-butoxide and finally into *n*-butene on HZ-5. Then, the formed *n*-butene can directly participate in the olefin-based cycle via the reaction with methanol and avoid an induction period of methanol conversion (Scheme 1, blue frame). Additionally, the continuous participation

Scheme 1. Proposed Reaction Pathway Containing the Dual-Cycle Mechanism of MTA Conversion before and after *n*-Butanol Cofeeding



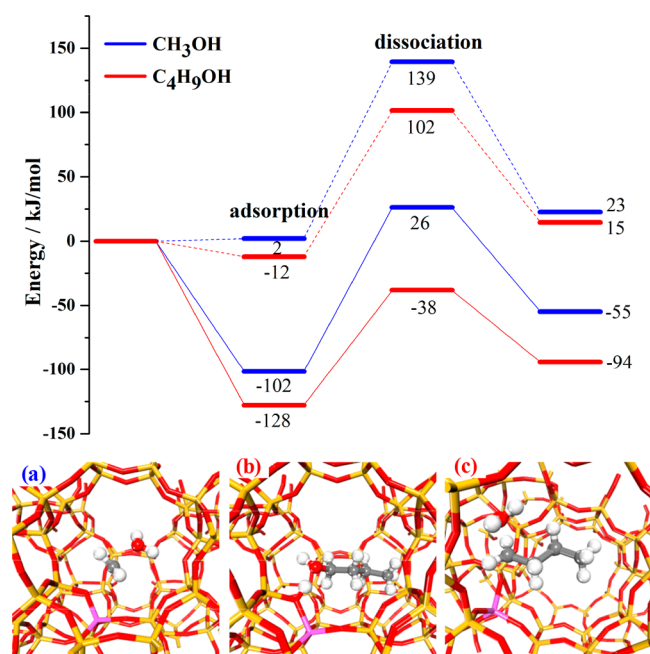


Figure 10. Gibbs free energy diagrams of the dissociation of methanol (in blue) and *n*-butanol (in red) in HZ-5 at 0 K (solid line) and 723 K (dash line). The structures of the adsorption of *n*-butanol (b) and the dissociation transition states of methanol (a) and *n*-butanol (c) are shown as well.

of *n*-butene, which is formed from *n*-butanol, can strongly increase the proportion of the olefin-based cycle and suppress the aromatic-based cycle during the MTA conversion. Therefore, the accumulation of large polycyclic aromatics during the MTA conversion is strongly suppressed with the *n*-butanol cofeeding, which is supported by the TGA (Figure 5), GC–MS (Figure 6), and UV/vis spectroscopy (Figure 7 and 8). As a result, a longer catalyst lifetime of up to 50 h can be achieved for the 4%Ga-HZ-5 model catalyst during the MTA conversion with cofeeding of *n*-butanol.

4. CONCLUSIONS

In the present work, Ga-modified nano H-ZSM-5 catalysts with different Ga loadings of 1–5% have been prepared and used for the MTA conversion. After Ga introduction, a highest selectivity to aromatics of 66.7% could be obtained, while the catalyst lifetime decreased distinctly. By cofeeding of *n*-butanol during the MTA conversion, a prolonged catalyst lifetime of up to TOS = 50 h can be achieved. To elucidate the reaction mechanism and the roles of *n*-butanol in the MTA conversion, several complementary methods, i.e., TGA, GC–MS, in situ UV/vis, and ^{71}Ga MAS NMR spectroscopy, were employed. The results obtained by these methods can be summarized as follows:

- (i) The MTA conversion on H-ZSM-5 catalysts starts with a short period dominated by the olefin-based cycle as monitored by in situ UV/vis. The intermediates formed by this cycle, i.e., dienes, can be rapidly converted to other larger intermediates, e.g., polymethylbenzenes and dienyl carbenium ions. Subsequently, the aromatic-based cycle starts and plays the dominating role in the MTA conversion. With the further progress of the MTA conversion, an accumulation of larger coke compounds, mostly polycyclic aromatics, occurred, which leads to a pore blocking and a coverage of the active sites. Both these effects, finally, cause the catalyst deactivation, as indicated by UV/vis, GC–MS, and ^{71}Ga MAS NMR.

- (ii) In the case of cofeeding with *n*-butanol, *n*-butene is preferentially formed, which can directly participate in the olefin-based cycle via the reaction with methanol. With the continuous participation of *n*-butene, the proportion of the olefin-based cycle in the dual-cycle mechanism is strongly increased, while the aromatic-based cycle mechanism and the accumulation of larger coke compounds are significantly suppressed, as supported by UV/vis and GC–MS results. Therefore, a significantly longer catalyst lifetime can be achieved.

■ ASSOCIATED CONTENT

Supporting Information

This material is available free of charge via the Internet at <http://pubs.acs.org/>. The Supporting Information is available free of charge on the ACS Publications website at DOI: 10.1021/acscatal.7b03457.

Additional catalyst characterization, TGA, and recyclability data (PDF)

■ AUTHOR INFORMATION

Corresponding Author

*E-mail: lild@nankai.edu.cn.

ORCID

Weili Dai: 0000-0001-5752-0662

Michael Hunger: 0000-0002-1870-2743

Landong Li: 0000-0003-0998-4061

Notes

The authors declare no competing financial interest.

■ ACKNOWLEDGMENTS

This work was supported by the National Natural Science Foundation of China (Grant No. 21722303, 21421001, 21673295), the Municipal Natural Science Foundation of Tianjin (16JCQNJC04900), and the National Key Research and Development Program of China (Grant No. 2016YFB0701100). Furthermore, M.H. thanks the Deutsche Forschungsgemeinschaft for financial support.

■ REFERENCES

- (1) Stöcker, M. In *Zeolite and Catalysis: Synthesis, Reactions and Applications*, 1st ed.; Čejka, J., Corma, A., Zones, S., Eds.; Wiley-VCH: Weinheim, Germany, 2010; Vol. 2, pp 687–711.
- (2) Olsbye, U.; Svelle, S.; Lillerud, K. P.; Wei, Z. H.; Chen, Y. Y.; Li, J. F.; Wang, J. G.; Fan, W. B. *Chem. Soc. Rev.* **2015**, *44*, 7155–7176.
- (3) Olsbye, U.; Svelle, S.; Bjørgen, M.; Beato, P.; Janssens, T. V. W.; Joensen, F.; Bordiga, S.; Lillerud, K. P. *Angew. Chem., Int. Ed.* **2012**, *51*, 5810–5831.
- (4) Hemelsoet, K.; Van der Mynsbrugge, J.; De Wispelaere, K.; Waroquier, M.; Van Speybroeck, V. *ChemPhysChem* **2013**, *14*, 1526–1545.
- (5) Ilias, S.; Bhan, A. *ACS Catal.* **2013**, *3*, 18–31.
- (6) Ilias, S.; Bhan, A. *J. Catal.* **2014**, *311*, 6–16.
- (7) Tian, P.; Wei, Y. X.; Ye, M.; Liu, Z. M. *ACS Catal.* **2015**, *5*, 1922–1938.
- (8) Dai, W. L.; Wang, C. M.; Dyballa, M.; Wu, G. J.; Guan, N. J.; Li, L. D.; Xie, Z. K.; Hunger, M. *ACS Catal.* **2015**, *5*, 317–326.
- (9) Chowdhury, A. D.; Houben, K.; Whiting, G. T.; Mokhtar, M.; Asiri, A. M.; Al-Thabaiti, A. A.; Basahel, S. N.; Baldus, M.; Weckhuysen, B. M. *Angew. Chem., Int. Ed.* **2016**, *55*, 15840–15845.
- (10) Liu, Y.; Muller, S.; Berger, D.; Jelic, J.; Reuter, K.; Tonigold, M.; Sanchez-Sanchez, M.; Lercher, J. *Angew. Chem.* **2016**, *128*, 5817–5820.
- (11) Shen, X. Q.; Kang, J. C.; Niu, W.; Wang, M. H.; Zhang, Q. H.; Wang, Y. *Catal. Sci. Technol.* **2017**, *7*, 3598–3612.

- (12) Jia, Y. M.; Wang, J. W.; Zhang, K.; Liu, S. B.; Chen, G. L.; Yang, Y. F.; Ding, C. M.; Liu, P. *Catal. Sci. Technol.* **2017**, *7*, 1776–1791.
- (13) Jia, Y. M.; Wang, J. W.; Zhang, K.; Feng, W.; Liu, S. B.; Ding, C. M.; Liu, P. *Microporous Mesoporous Mater.* **2017**, *247*, 103–115.
- (14) Miyake, K.; Hirota, Y.; Ono, K.; Uchida, Y.; Tanaka, S.; Nishiyama, N. *J. Catal.* **2016**, *342*, 63–66.
- (15) Zhang, J. G.; Qian, W. Z.; Kong, C. Y.; Wei, F. *ACS Catal.* **2015**, *5*, 2982–2988.
- (16) Ono, Y. *Catal. Rev.: Sci. Eng.* **1992**, *34*, 179–226.
- (17) Seddon, D. *Catal. Today* **1990**, *6*, 351–372.
- (18) Yao, J.; le van Mao, R.; Dufresne, L. *Appl. Catal.* **1990**, *65*, 175–188.
- (19) Svelle, S.; Joensen, F.; Nerlov, J.; Olsbye, U.; Lillerud, K. P.; Kolboe, S.; Bjørgen, M. J. *Am. Chem. Soc.* **2006**, *128*, 14770–14771.
- (20) Bjørgen, M.; Svelle, S.; Joensen, F.; Nerlov, J.; Kolboe, S.; Bonino, F.; Palumbo, L.; Bordiga, S.; Olsbye, U. *J. Catal.* **2007**, *249*, 195–207.
- (21) Ono, Y.; Adachi, H.; Senoda, Y. *J. Chem. Soc., Faraday Trans. 1* **1988**, *84*, 1091–1099.
- (22) Inoue, Y.; Nakashiro, K.; Ono, Y. *Microporous Mater.* **1995**, *4*, 379–383.
- (23) Freeman, D.; Wells, R. P. K.; Hutchings, G. J. *Chem. Commun.* **2001**, 1754–1755.
- (24) Freeman, D.; Wells, R. P. K.; Hutchings, G. J. *J. Catal.* **2002**, *205*, 358–365.
- (25) Freeman, D.; Wells, R. P. K.; Hutchings, G. J. *Catal. Lett.* **2002**, *82*, 217–225.
- (26) Conte, M.; Lopez-Sanchez, J. A.; He, Q.; Morgan, D. J.; Ryabenkova, Y.; Bartley, J. K.; Carley, A. F.; Taylor, S. H.; Kiely, C. J.; Khalid, K.; Hutchings, G. J. *Catal. Sci. Technol.* **2012**, *2*, 105–112.
- (27) Lopez-Sanchez, J. A.; Conte, M.; Landon, P.; Zhou, W.; Bartley, J. K.; Taylor, S. H.; Carley, A. F.; Kiely, C. J.; Khalid, K.; Hutchings, G. J. *Catal. Lett.* **2012**, *142*, 1049–1056.
- (28) Niu, X. J.; Gao, J.; Miao, Q.; Dong, M.; Wang, G. F.; Fan, W. B.; Qin, Z. F.; Wang, J. G. *Microporous Mesoporous Mater.* **2014**, *197*, 252–261.
- (29) Wilson, S.; Barger, P. *Microporous Mesoporous Mater.* **1999**, *29*, 117–126.
- (30) Dahl, I. M.; Mostad, H.; Akporiaye, D.; Wendelbo, R. *Microporous Mesoporous Mater.* **1999**, *29*, 185–190.
- (31) Djieugoue, M. A.; Prakash, A. M.; Kevan, L. *J. Phys. Chem. B* **2000**, *104*, 6452–6461.
- (32) Dai, W. L.; Wang, X.; Wu, G. J.; Li, L. D.; Guan, N. J.; Hunger, M. *ChemCatChem* **2012**, *4*, 1428–1435.
- (33) Dai, W. L.; Cao, G.; Yang, L.; Wu, G. J.; Dyballa, M.; Hunger, M.; Guan, N. J.; Li, L. D. *Catal. Sci. Technol.* **2017**, *7*, 607–618.
- (34) Losch, P.; Boltz, M.; Bernardon, C.; Louis, B.; Palcic, A.; Valtchev, V. *Appl. Catal., A* **2016**, *509*, 30–37.
- (35) Inagaki, S.; Sato, K.; Hayashi, S.; Tatami, J.; Kubota, Y.; Wakihara, T. *ACS Appl. Mater. Interfaces* **2015**, *7*, 4488–4493.
- (36) Deng, Y. Q.; Zhou, W. F.; Lv, H. M.; Zhang, Y. Y.; Au, C. T.; Yin, S.-F. *RSC Adv.* **2014**, *4*, 37296–37301.
- (37) Choi, M.; Na, K.; Kim, J.; Sakamoto, Y.; Terasaki, O.; Ryoo, R. *Nature* **2009**, *461*, 246–249.
- (38) Iwakai, K.; Tago, T.; Konno, H.; Nakasaka, Y.; Masuda, T. *Microporous Mesoporous Mater.* **2011**, *141*, 167–174.
- (39) Shen, K.; Wang, N.; Qian, W. Z.; Cui, Y.; Wei, F. *Catal. Sci. Technol.* **2014**, *4*, 3840–3844.
- (40) Wang, N.; Qian, W. Z.; Shen, K.; Su, C.; Wei, F. *Chem. Commun.* **2016**, *52*, 2011–2014.
- (41) Lai, P. C.; Chen, C. H.; Hsu, H. Y.; Lee, C. H.; Lin, Y. C. *RSC Adv.* **2016**, *6*, 67361–67371.
- (42) Kim, J.; Choi, M.; Ryoo, R. *J. Catal.* **2010**, *269*, 219–228.
- (43) Milina, M.; Mitchell, S.; Crivelli, P.; Cooke, D.; Perez-Ramirez, J. *Nat. Commun.* **2014**, *5*, 3922.
- (44) Milina, M.; Mitchell, S.; Cooke, D.; Crivelli, P.; Perez-Ramirez, J. *Angew. Chem., Int. Ed.* **2015**, *54*, 1591–1594.
- (45) Sun, X. Y.; Mueller, S.; Liu, Y.; Shi, H.; Haller, G. L.; Sanchez-Sanchez, M.; van Veen, A. C.; Lercher, J. A. *J. Catal.* **2014**, *317*, 185–197.
- (46) Kresse, G.; Furthmüller, J. *Phys. Rev. B: Condens. Matter Mater. Phys.* **1996**, *54*, 11169–11181.
- (47) Henkelman, G.; Jonsson, H. *J. Chem. Phys.* **1999**, *111*, 7010–7022.
- (48) Wellendorff, J.; Lundgaard, K.; Mogelhoff, A.; Petzold, V.; Landis, D.; Norskov, J.; Bligaard, T.; Jacobsen, K. *Phys. Rev. B: Condens. Matter Mater. Phys.* **2012**, *85*, 235149.
- (49) Dai, W. L.; Wang, C. M.; Yi, X. F.; Zheng, A. M.; Li, L. D.; Wu, G. J.; Guan, N. J.; Xie, Z. K.; Dyballa, M.; Hunger, M. *Angew. Chem., Int. Ed.* **2015**, *54*, 8783–8786.
- (50) Wang, C. M.; Wang, Y. D.; Du, Y. J.; Yang, G.; Xie, Z. K. *Catal. Sci. Technol.* **2016**, *6*, 3279–3288.
- (51) Treacy, M. M. J.; Higgins, J. B. *Collection of Simulated XRD Powder Patterns for Zeolites*, 5th revised ed.; Elsevier: Amsterdam, Netherlands, 2007.
- (52) Jiang, Y.; Huang, J.; Dai, W.; Hunger, M. *Solid State Nucl. Magn. Reson.* **2011**, *39*, 116–141.
- (53) Prasad, S.; Petrov, M. *Solid State Nucl. Magn. Reson.* **2013**, *54*, 26–31.
- (54) Dai, W. L.; Wang, C. M.; Tang, B.; Wu, G. J.; Guan, N. J.; Xie, Z. K.; Hunger, M.; Li, L. D. *ACS Catal.* **2016**, *6*, 2955–2964.
- (55) Szeto, K. C.; Gallo, A.; Hernández-Morejudo, S.; Olsbye, U.; De Mallmann, A.; Lefebvre, F.; Gauvin, R. M.; Delevoye, L.; Scott, S. L.; Taoufik, M. *J. Phys. Chem. C* **2015**, *119*, 26611–26619.
- (56) Hunger, M. *Solid State Nucl. Magn. Reson.* **1996**, *6*, 1–29.
- (57) Serykh, A. I. *Chem. Phys. Lett.* **2012**, *554*, 159–162.
- (58) Xia, H. A.; Sun, K. Q.; Fan, F. T.; Sun, K. J.; Su, W. J.; Feng, Z. C.; Ying, P. L.; Li, C. J. *Catal.* **2008**, *259*, 269–275.
- (59) Arnold, A.; Steuernagel, S.; Hunger, M.; Weitkamp, J. *Microporous Mesoporous Mater.* **2003**, *62*, 97–106.
- (60) Zheng, B.; Hua, W.; Yue, Y.; Gao, Z. *J. Catal.* **2005**, *232*, 143–151.
- (61) Al-Yassir, N.; Akhtar, M. N.; Al-Khattaf, S. *J. Porous Mater.* **2012**, *19*, 943–960.
- (62) Li, Z. L.; Lepore, A. W.; Salazar, M. F.; Foo, G. S.; Davison, B. H.; Wu, Z. L.; Narula, C. K. *Green Chem.* **2017**, *19*, 4344–4352.
- (63) Dai, W. L.; Sun, X. M.; Tang, B.; Wu, G. J.; Li, L. D.; Guan, N. J.; Hunger, M. *J. Catal.* **2014**, *314*, 10–20.
- (64) Dai, W. L.; Wang, X.; Wu, G. J.; Guan, N. J.; Hunger, M.; Li, L. D. *ACS Catal.* **2011**, *1*, 292–299.
- (65) Dai, W. L.; Wu, G. J.; Li, L. D.; Guan, N. J.; Hunger, M. *ACS Catal.* **2013**, *3*, 588–596.
- (66) Qi, L.; Li, J. Z.; Wei, Y. X.; Xu, L.; Liu, Z. M. *Catal. Sci. Technol.* **2016**, *6*, 3737–3744.
- (67) Wang, C. M.; Wang, Y. D.; Xie, Z. K. *J. Catal.* **2013**, *301*, 8–19.